THE JOURNAL OF PHYSICAL CHEMISTRY A
A JOURNAL OF THE AMERICAN CHEMICAL SOCIETY

pubs.acs.org/JPCA Article

Millimeter-Wave and High-Resolution Infrared Spectroscopy of 3-Furonitrile

Published as part of The Journal of Physical Chemistry A virtual special issue "Richard J. Saykally Festschrift".

William H. Styers, Maria A. Zdanovskaia, Brian J. Esselman, Andrew N. Owen, Samuel M. Kougias, Brant E. Billinghurst, Jianbao Zhao, Robert J. McMahon,* and R. Claude Woods*

Cite This: https://doi.org/10.1021/acs.jpca.4c03093 Read Online

ACCESS | Metrics & More | Article Recommendations | Supporting Information

ABSTRACT: The rotational spectrum of 3-furonitrile has been collected from 85 to 500 GHz, spanning the most intense rotational transitions observable at room temperature. The large dipole moment imparted by the nitrile substituent confers substantial intensity to the rotational spectrum, enabling the observation of over 5600 new rotational transitions. Combined with previously published transitions, the available data set was least-squares fit to partial-octic, distorted-rotor A- and S-reduced Hamiltonian models with low statistical uncertainty (σ_{fit} < 0.031 MHz) for the ground vibrational state. Similar to its isomer 2-furonitrile, the two lowest-energy vibrationally excited states of 3-furonitrile (ν_{17}, ν_{24}), which correspond to the in-plane and out-of-plane nitrile bending vibrations, form an *a*- and *b*-axis Coriolis-coupled dyad. Rotationally resolved infrared transitions (30−600 cm^{-1}) and over 4200 pure rotational transitions for both ν_{17} and ν_{24} were fit to a partial-octic, Coriolis-coupled, two-state Hamiltonian with low statistical uncertainty (σ_{fit} rot < 0.045 MHz, σ_{fit} IR < 6.1 MHz). The least-squares fitting of these vibrationally excited states provides their accurate and precise vibrational frequencies (ν_{17} = 168.193 164 8 (67) cm^{-1} and ν_{24} = 169.635 831 5 (77) cm^{-1}) and seven Coriolis-coupling terms (G_a, G_a^J, G_a^K, F_{bc}, F_{bc}^K, G_b, and F_{ac}). The two fundamental states exhibit a notably small energy gap (1.442 667 (10) cm^{-1}) and an inversion of the relative energies of ν_{17} and ν_{24} compared to those of the isomer 2-furonitrile. The rotational frequencies and spectroscopic constants of 3-furonitrile that we present herein provide a sufficient basis for conducting radioastronomical searches for this molecule across the majority of the frequency range available to current radiotelescopes.

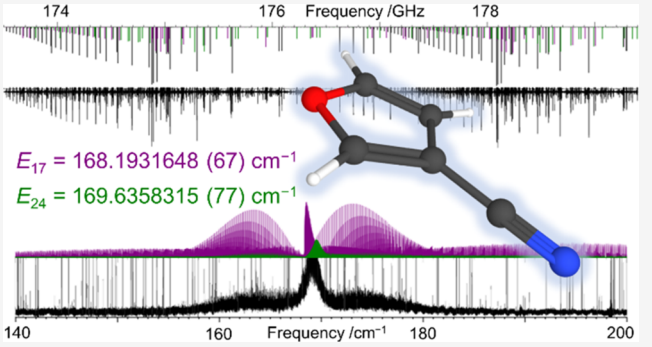

INTRODUCTION

Despite the availability of precise and accurate laboratory rotational spectra for many aromatic heterocycles with a permanent dipole moment, all radioastronomical searches for aromatic heterocycles have been unsuccessful.[1−9] Detection of furan is of particular interest to astrochemists and astrobiologists as a fundamental organic molecule and as a molecule that bears structural resemblance to the furanose sugars found in DNA and RNA. As a result, furan has been the target of several published astronomical searches.[6−9] The detection of any molecule by radioastronomy is dependent on its abundance (column density) in the source and the intensity of its transitions (proportional to the square of its permanent dipole moment). In the case of furan, the permanent dipole moment is small (μ_a = 0.685 (1) D)[10] compared to its nitrile-containing derivatives (measured μ_a = 4.51 (2) D and μ_b = 0.901 (5) D for 2-furonitrile;[11,12] computed μ_a = 3.78 D and μ_b = 0.40 D for 3-furonitrile[12,13]). In a theoretical study, Simbizi *et al.*[14] reported the structures, spectroscopic constants, and proton affinities of furan and its nitrile derivatives, 2- and 3-furonitrile, in conditions relevant to the interstellar medium (ISM). They also provided theoretical spectroscopic constants for the protonated forms of 2- and 3-furonitrile, offering an additional avenue for the detection of nitrile derivatives of furan in extraterrestrial conditions. Inspired, in part, by recent astronomical detections of aromatic nitriles, *e.g.*, benzonitrile,[8] 2-cyanonaphthalene,[15] 3-cyanonaphthalene,[15] and 2-cyanoindene,[16] there have been several recent reports of the laboratory rotational spectra of nitrile-substituted heteroaromatic molecules.[13,17−29] These nitrile-substituted heteroaromatics, or their protonated forms, may serve as valuable tracer molecules for their corresponding

Received: May 10, 2024
Revised: June 8, 2024
Accepted: June 10, 2024
Published: June 25, 2024

elusive unsubstituted species, as well as being important targets of astronomical searches themselves.

Rotational spectra of 2- and 3-furonitrile (Figure 1) have been reported previously.[11,13,29,30] The dipole moment of 2-furonitrile, determined by Stark shift,[11] and its nuclear quadrupole coupling constants[30] were reported in studies of the rotational spectrum up to 40 GHz. Two contemporaneous works (1) by our group (up to 750 GHz)[29] and (2) by Melosso *et al.* (up to 330 GHz)[13] expanded the frequency coverage and improved the determination of the spectroscopic constants of 2-furonitrile. In addition to the ground vibrational state, the former study investigated the three lowest-energy vibrationally excited states and incorporated high-resolution infrared (IR) spectral data in the analysis.[29] The latter study improved the determination of the nuclear quadrupole coupling constants and determined a partial semi-experimental equilibrium structure (r_e^{SE}) from the rotational constants of the normal and all heavy-atom substituted isotopologues.[13] In contrast to the thorough study of 2-furonitrile, the only previous investigation of the rotational spectrum of 3-furonitrile was recently provided by Melosso *et al.*[13] As with their study of 2-furonitrile, the nuclear quadrupole coupling constants and a partial r_e^{SE} structure were reported. Herein, we provide an updated analysis of the ground vibrational state of 3-furonitrile incorporating all previous measurements[13] and, for the first time, provide an analysis of the two lowest-energy vibrationally excited states, incorporating both high-resolution IR and millimeter-wave spectra. As is the case for other aromatic nitriles,[22−29] these two vibrational modes form a Coriolis-coupled dyad, and their vibrational energies are accurately determined as a result of this analysis. Additionally, we update the least-squares fit of the ground vibrational state of 2-furonitrile to include all currently available microwave transitions.[11,13,30] The combined transition data sets and the improved spectroscopic constants provide the best available foundation for future radioastronomical searches of both molecules.

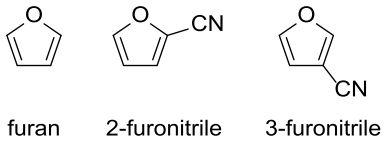

Figure 1. Furan and its two singly substituted nitrile derivatives, 2- and 3-furonitrile.

EXPERIMENTAL METHODS

A commercial sample of 3-furonitrile (97% purity) was used without purification for all spectroscopic measurements. Using a millimeter-wave spectrometer that has been previously described,[26,31,32] the rotational spectrum of 3-furonitrile was collected from 85 to 125, from 140 to 230, and from 235 to 500 GHz, in a continuous flow at room temperature, with sample pressures of 3−15 mTorr. The complete spectrum from 85 to 500 GHz was obtained automatically over approximately eight days, given the following experimental parameters: 0.6 MHz/s sweep rate, 10 ms time constant, and 50 kHz AM and 500 kHz FM modulation in a tone-burst design. A uniform frequency measurement uncertainty of 0.050 MHz was assumed for all measurements.

High-resolution infrared data presented in this work were recorded at the Canadian Light Source (CLS) Synchrotron far-IR beamline using a Bruker IFS 125 HR Spectrometer, with synchrotron radiation and a 9.4-m optical path length difference providing a nominal resolution of 0.00096 cm^{-1}. The cell is a 2-m, White-type multipass cell; the total path length is 72 m. Spectra were collected at room temperature at a series of pressures for the analysis of various vibrational states, which have different infrared intensities. In the range from 30 to 600 cm^{-1}, spectra were collected at 0.0191, 0.123, and 0.481 Torr using a 6-μm Mylar beamsplitter, 50-μm polypropylene cell windows, and a superconducting niobium TES bolometer detector. Data collection times were all 18 h or less. The aperture was 1.5 mm, and the preamplifier gain of the detector was set to 6×. In the range from 30 to 300 cm^{-1}, spectra were collected at 0.060 and 0.0647 Torr using a 6-μm Mylar beamsplitter, 50-μm polypropylene cell windows, and a superconducting niobium TES bolometer detector. The aperture was 1.5 mm, and the preamplifier gain of the detector was set to 10×. Several of the spectra used a 300 cm^{-1} low-pass filter. A uniform frequency measurement uncertainty of 0.00018 cm^{-1} (∼6 MHz) was assumed for all infrared measurements.

The separate segments of the rotational spectrum were combined into a single broadband spectrum using Kisiel's Assignment and Analysis of Broadband Spectra (AABS) software.[33,34] The AABS software suite was used to analyze both the rotational and high-resolution infrared spectra. Pickett's SPFIT/SPCAT[35] was used for least-squares fitting and spectral predictions, along with Kisiel's PIFORM, PLANM, and AC programs for analysis.[36]

COMPUTATIONAL METHODS

Electronic structure calculations were carried out with Gaussian 16[37] using the WebMO interface[38] to obtain theoretical spectroscopic constants. Optimized geometries at the B3LYP/6-311+G(2d,p) and MP2/6-311+G(2d,p) levels were obtained using "verytight" convergence criteria and an "ultrafine" integration grid, and subsequent anharmonic vibrational frequency calculations were carried out. Additional electronic structure calculations were carried out using a development version of CFOUR[39] to obtain an optimized structure at the CCSD(T)/cc-pCVTZ level of theory, including core electrons. The optimized geometry and the same level of theory were subsequently used for an anharmonic, second-order vibrational perturbation theory (VPT2) calculation, wherein cubic force constants are evaluated by numerical differentiation of analytic first derivatives at displaced points.[40−42] Computational output files can be found in the Supporting Information.

RESULTS AND DISCUSSION

Spectral Analysis. 3-Furonitrile is a prolate, asymmetric top (C_s, κ = −0.913, Figure 2) with a substantial permanent dipole

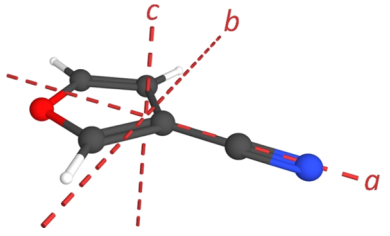

Figure 2. 3-Furonitrile structure (C_s, μ_a = 3.78 D and μ_b = 0.40 D, CCSD(T))[13] with principal inertial axes.

https://doi.org/10.1021/acs.jpca.4c03093
J. Phys. Chem. A XXXX, XXX, XXX−XXX

moment along the *a*-axis and a smaller dipole moment along the *b*-axis (μ_a = 3.78 D and μ_b = 0.40 D, CCSD(T)[13]). As a result, the *a*-type transitions are much more intense than the *b*-type transitions, and the former dominate most of the predicted rotational spectrum up to 700 GHz (Figure 3). The *b*-type transitions are expected to be the main spectral feature only at frequencies above 550 GHz.

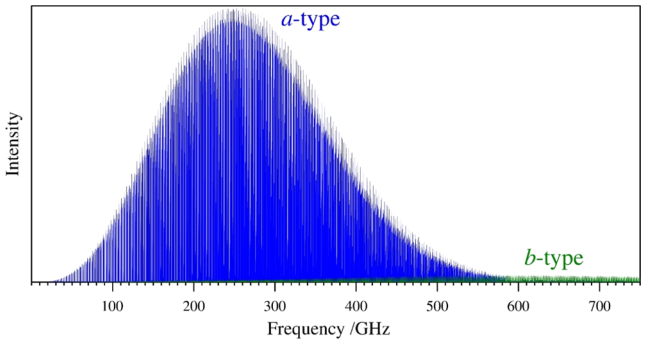

Figure 3. Predicted rotational spectrum (SPCAT) of the ground vibrational state of 3-furonitrile to 750 GHz at 295 K. The measured frequency range in this work is from 85 to 500 GHz.

Considering the low intensity of the *b*-type transitions and the generally poorer signal-to-noise ratio of our instrument in the frequency region above 550 GHz, we collected the rotational spectrum of 3-furonitrile only to 500 GHz. This upper limit contrasts with that of our earlier study of 2-furonitrile, whose larger *b*-axis dipole component (μ_b = 0.7 D) made it possible to glean useful data from a higher-frequency spectral range.[29] Extending the measured frequency range for 3-furonitrile to lower frequency (85−125 GHz) was quite valuable in obtaining a reasonable least-squares fit of the vibrationally excited states, due to the intense state-mixing that begins to appear even at moderate values of *J* and *K* (*vide infra*). The full frequency range studied in this work enables the measurement of the majority of the most intense transitions populated at ambient temperature (Figure 3). As shown in Figure 4, the rotational spectrum of 3-furonitrile in the observed millimeter-wave frequency range is defined by the typical oblate-type, R-branch bands observed for other cyano-substituted arenes in similar frequency ranges.[13,22−29] The *b*-type transitions are approximately 100 times weaker than the *a*-type transitions and are thus substantially weaker than the *a*-type R-branch transitions of even many of the vibrationally excited states, including ν_{17} and ν_{24} (*vide infra*).

Ground-State Spectrum of 3-Furonitrile. For the ground vibrational state of 3-furonitrile, the spectral density and frequency range observed allow for the measurement, assignment, and least-squares fitting of over 5800 independent transitions in the combined data set. Melosso *et al.*[13] reported over 1350 transitions of 3-furonitrile between 6 and 22 GHz, outside the frequency coverage of this work, and from 240 to 320 GHz, overlapping with this work. Taken together, the available spectra of 3-furonitrile include transitions with J'' + 1 up to 154 and K_a'' up to 49 for the ground vibrational state. The smaller range of quantum numbers for observed transitions of 3-furonitrile, relative to 2-furonitrile (J'' + 1 up to 190 and K_a'' up to 59), is in line with the reduced spectral coverage relative to 2-furonitrile.[29] The number of measured transitions in this work is decreased by about 30% relative to 2-furonitrile due to the combined impact of the smaller frequency coverage and the reduced *b*-type dipole, which allowed the measurement of only a small number of *b*-type transitions.

The combined transition data set (Figure 5) for 3-furonitrile was least-squares fit to a partial-octic, centrifugally distorted-rotor Hamiltonian with and without nuclear quadrupole coupling. The resulting spectroscopic constants in the A and S reductions, and I′ representation are provided in Table 1. The least-squares fit without nuclear quadrupole coupling includes only the transitions newly measured in this work. The least-squares fit with nuclear quadrupole coupling includes all available transitions using the reported nominal measurement uncertainty. In cases where transitions between 240 and 320 GHz were duplicated in the data set between this and the previous work,[13] the transition frequency with the smallest *obs.* − *calc.* value was used. From this work only, over 5600 transitions were least-squares fit (σ_{fit} = 0.031 MHz); the combined data set contains over 5800 transitions (σ_{fit} = 0.030

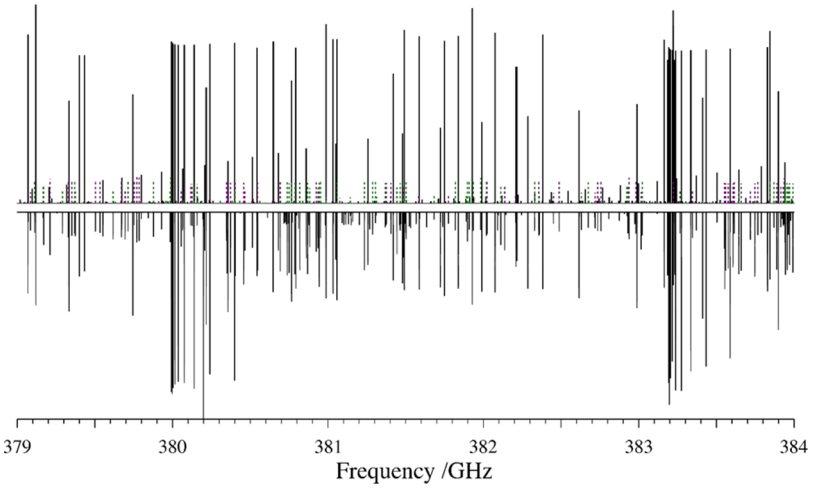

Figure 4. Predicted (top) and experimental (bottom) rotational spectra of 3-furonitrile from 379 to 384 GHz. Ground-state transitions of 3-furonitrile for the J'' + 1 = 118 and J'' + 1 = 119 bands appear in black. The high-K_a portions of two R-branch series (J'' + 1 = 107 and 108) are visible moving across the spectral range from high to low frequency. Transitions for ν_{17} are in purple, and transitions for ν_{24} are in green. Unidentified transitions are attributable to higher-energy vibrationally excited states of 3-furonitrile.

https://doi.org/10.1021/acs.jpca.4c03093
J. Phys. Chem. A XXXX, XXX, XXX−XXX

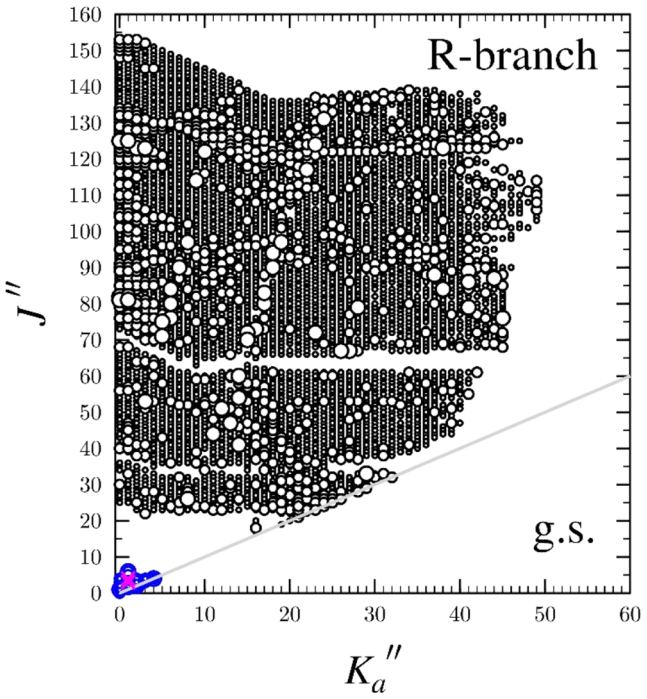

Figure 5. Data distribution plot for the least-squares fit of spectroscopic data for the vibrational ground state of 3-furonitrile. The size of the symbol is proportional to the value of $|(f_{obs.} - f_{calc.})/\delta f|$, where δf is the frequency measurement uncertainty, and all quotient values are smaller than 3. Black circles represent millimeter-wave data, while blue (R-branch) and pink (P-branch) symbols represent microwave data from Melosso *et al.*[13]

MHz). In the least-squares fit without quadrupole coupling, all of the on-diagonal octic centrifugal distortion terms, excluding L_K, were determined satisfactorily in both reductions. Values for the octic terms not included in the least-squares fit were held constant at zero, as no currently available software package can predict these values. For the combined data set, hyperfine-resolved transitions were observed only below 22 GHz. These transitions provided the sole information used in determining the nuclear quadrupole coupling constants, but they were not included in the determination of the octic centrifugal distortion constants. A few of the sextic and octic distortion constants (L_J and L_{JJK} in the S reduction and Φ_J in the A reduction) in the combined data set became undeterminable. As a result, these parameters were held constant at their corresponding values determined in the least-squares fit without quadrupole coupling (using only newly measured transitions in this work).

The agreement of the spectroscopic constants determined by the least-squares fit using only data from this work, by the least-squares fit incorporating all available data, and by Melosso *et al.*[13] is generally quite satisfactory. The spectroscopic constants appear to be best determined in the combined data set. Interestingly, the broader frequency coverage in this work necessitated the inclusion of only two additional octic centrifugal distortion constants compared to the previous work. The computed CCSD(T)/cc-pCVTZ spectroscopic constants are in generally good agreement with their corresponding experimental values of the combined work with the notable exceptions of h_1, Φ_J, and ϕ_J. As expected, the rotational constants are predicted within 0.5% of their experimental values using this level of theory and basis set. The computed quartic distortion constants are within 14% of their experimental values. With the aforementioned exceptions of h_1, Φ_J, and ϕ_J, the sextic centrifugal distortion constants are likewise predicted within 22% of the experimental values. The experimental value of h_1, however, is approximately half of its computed value, while the value of ϕ_J is nearly twice its computed value. In a more extreme deviation, the experimental value of Φ_J is nearly equal in magnitude but opposite in sign to its computed value. Given the extensive frequency and J/K range of the current data set, the experimental centrifugal distortion constants need to model significant levels of centrifugal distortion. It is likely that untreated, higher-order centrifugal distortion is impacting these constants. This notion is supported by analysis presented in the 2-furonitrile study and will be discussed further below. Attempts to hold these problematic constants at their computed values resulted in large increases in the σ values of the least-squares fits and poor modeling of many transitions. Attempts to use additional octic centrifugal distortion constants were unsuccessful in improving the least-squares fit. As a result, the above-mentioned octic parameters with large discrepancies from their computed values are included in the least-squares fits and should be considered somewhat empirical. For comparison, computed spectroscopic constants at the B3LYP/6-311+G(2d,p) and MP2/6-311+G(2d,p) levels are provided in the Supporting Information.

Coriolis-Coupled Dyad of ν_{17} and ν_{24}. The two lowest-energy vibrationally excited states of 3-furonitrile are the in-plane (ν_{17}, A', ~168 cm^{-1}) and out-of-plane (ν_{24}, A'', ~170 cm^{-1}) bending modes of the nitrile group (Figure 6). Like the other cyanoarenes,[22−29] energetic proximity and symmetry of these states enable strong *a*- and *b*-axis Coriolis coupling and substantial state-mixing. The resulting perturbation of transition frequencies is evident throughout the rotational and infrared spectra observed in this work. These two types of spectra are complementary, but in this work, transitions of the rotational spectra were available first and initially easier to assign and least-squares fit. As is evident in Figure 7, not only does ν_{24} have a much lower far-IR intensity, but the two fundamental states are so close in energy that the ν_{24} transitions are tucked in among the ν_{17} transitions. The millimeter-wave transitions, however, are comparable in intensity and readily predicted using computed vibration−rotation interaction constants, computed G_a constant from the Coriolis $|\zeta^a_{17,24}|$ constant, and the ground-state experimental spectroscopic constants. Initially, the G_b constant was not included in the least-square fitting model, due to the very small computed $|\zeta^b_{17,24}|$ value, but in later stages, it had to be incorporated into the analysis. While the millimeter-wave analysis is sufficient to determine the accurate and precise energy separation between these two states, rotationally resolved infrared spectra are required to accurately determine their individual band origins. With the infrared intensity of ν_{24} less than half that of ν_{17} (Figure 7) and with the very close band origins for these two states (Figures 6 and 7), having a preliminary fit of the rotational data made the measurement, assignment, and least-squares fitting of these states in the IR spectrum much more straightforward.

In total, over 4200 rotational transitions for each vibrational state, over 725 rotationally resolved infrared transitions for ν_{17}, and 150 rotationally resolved infrared transitions for ν_{24} were least-squares fit to a two-state, Coriolis-coupled, partial-octic, centrifugally distorted-rotor Hamiltonian model in the I^r representation. Transitions ranging in $J'' + 1$ from 23 to 154 and in K_a'' from 0 to 40 were assigned and least-squares fit for

https://doi.org/10.1021/acs.jpca.4c03093
J. Phys. Chem. A XXXX, XXX, XXX−XXX

Table 1. Experimental and Computational Spectroscopic Constants for the Ground Vibrational State of 3-Furonitrile (S- and A-Reduced Hamiltonian, I^r Representation)

	S reduction, I^r representation				A reduction, I^r representation		
	experimental (this work only)	experimental (combined)[a,b]	CCSD(T)[c]		experimental (this work only)	experimental (combined)[a,b]	CCSD(T)[c]
A_0 (MHz)	9296.55275 (56)	9296.54865 (11)	9261	A_0 (MHz)	9296.55253 (57)	9296.54864 (11)	9261
B_0 (MHz)	1940.266596 (34)	1940.266379 (11)	1930	B_0 (MHz)	1940.269840 (35)	1940.269661 (11)	1930
C_0 (MHz)	1604.631704 (33)	1604.631922 (10)	1596	C_0 (MHz)	1604.628513 (34)	1604.628704 (11)	1596
D_J (kHz)	0.0547100 (30)	0.05471374 (92)	0.0525	Δ_J (kHz)	0.0728679 (34)	0.07287264 (78)	0.0700
D_{JK} (kHz)	2.963541 (51)	2.963571 (34)	2.95	Δ_{JK} (kHz)	2.854516 (49)	2.854619 (35)	2.84
D_K (kHz)	0.4246 (13)	0.41496 (40)	0.368	Δ_K (kHz)	0.5153 (13)	0.50570 (40)	0.456
d_1 (kHz)	−0.0133901 (14)	−0.01337876 (44)	−0.0127	δ_J (kHz)	0.0133908 (14)	0.01338134 (49)	0.0127
d_2 (kHz)	−0.00908308 (69)	−0.00908410 (40)	−0.00875	δ_K (kHz)	1.62865 (12)	1.628774 (69)	1.59
H_J (Hz)	−0.00003372 (19)	−0.000033605 (28)	−0.0000297	Φ_J (Hz)	−0.00000288 (21)	[−0.00000288]	0.0000024
H_{JK} (Hz)	0.0045131(27)	0.0045117 (17)	0.00441	Φ_{JK} (Hz)	0.0066573 (64)	0.0066727 (57)	0.00650
H_{KJ} (Hz)	−0.038343 (51)	−0.038231 (36)	−0.0387	Φ_{KJ} (Hz)	−0.046046 (54)	−0.045962 (40)	−0.0462
H_K (Hz)	0.04558 (98)	0.03850 (43)	0.0359	Φ_K (Hz)	0.05096 (99)	0.04385 (44)	0.0412
h_1 (Hz)	−0.000000761 (43)	−0.000001063 (17)	−0.0000020	ϕ_J (Hz)	0.000002384 (47)	0.000002150 (23)	0.0000011
h_2 (Hz)	0.000015800 (29)	0.000015826 (19)	0.0000161	ϕ_{JK} (Hz)	0.0031021 (51)	0.0031021 (31)	0.00326
h_3 (Hz)	0.000003210 4 (80)	0.0000032260 (72)	0.0000031	ϕ_K (Hz)	0.05430 (17)	0.05450 (15)	0.0542
L_J (mHz)	0.0000001532 (43)	[0.000000153]		L_J (mHz)	0.0000001704 (44)	0.0000001751 (12)	
L_{JJK} (mHz)	−0.000010887 (78)	[−0.0000109]		L_{JJK} (mHz)	−0.000012769 (78)	−0.000013130 (64)	
L_{JK} (mHz)	0.0001478 (12)	0.00015280 (92)		L_{JK} (mHz)	0.0001036 (12)	0.00010911 (94)	
L_{KKJ} (mHz)	−0.001436 (17)	−0.001518 (13)		L_{KKJ} (mHz)	−0.001274 (17)	−0.001360 (13)	
3/2 χ_{aa} (MHz)		−6.33793 (70)	−6.588[d]			−6.33791 (70)	−6.588[d]
$(\chi_{bb} - \chi_{cc})/4$ (MHz)		0.15787 (25)	0.159[d]			0.15786 (25)	0.159[d]
Δ_i (uÅ^2)[e]	0.119329 (9)	0.119233 (3)	0.283		0.120389 (9)	0.120305 (3)	0.283
N_{lines}[f]	5655	5894			5655	5894	
σ_{fit} (MHz)	0.031	0.031			0.031	0.031	

[a]Includes transitions from previous work.[13] [b]Parameters in brackets that could not be determined were held constant at the value determined using data from this work only. [c]Evaluated with the cc-pCVTZ basis set. [d]Value from previous work.[13] [e]Inertial defect, $\Delta_i = I_c - I_a - I_b$, calculated using PLANM from the B_0 constants. [f]Number of fitted transition frequencies.

https://doi.org/10.1021/acs.jpca.4c03093
J. Phys. Chem. A XXXX, XXX, XXX−XXX

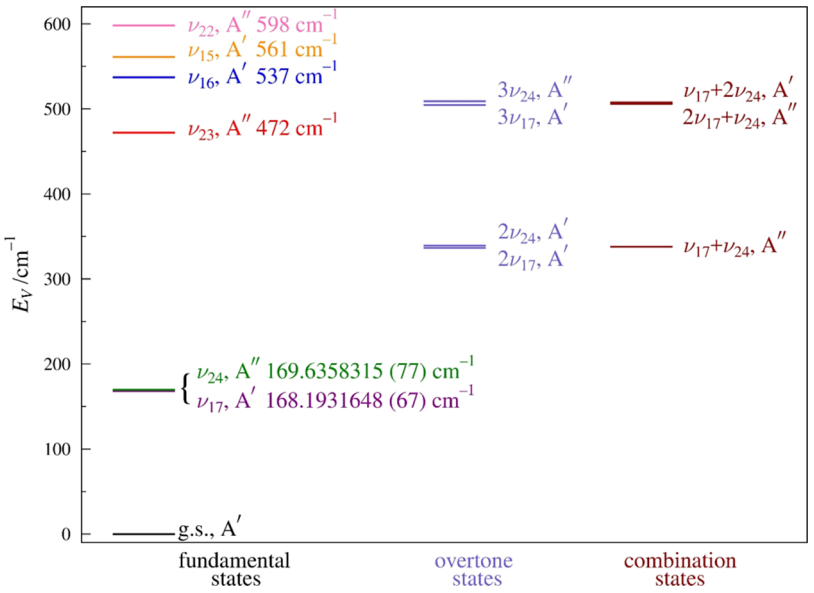

Figure 6. Vibrational energy levels of 3-furonitrile below 620 cm^{-1}. The energy values of ν_{17} (purple) and ν_{24} (green) result from the experimental analysis presented herein. Higher-energy fundamental-state energies are from previous gas-phase experimental measurements,[43] and overtone- and combination-state energies are extrapolated from the experimentally measured energies of the current work.

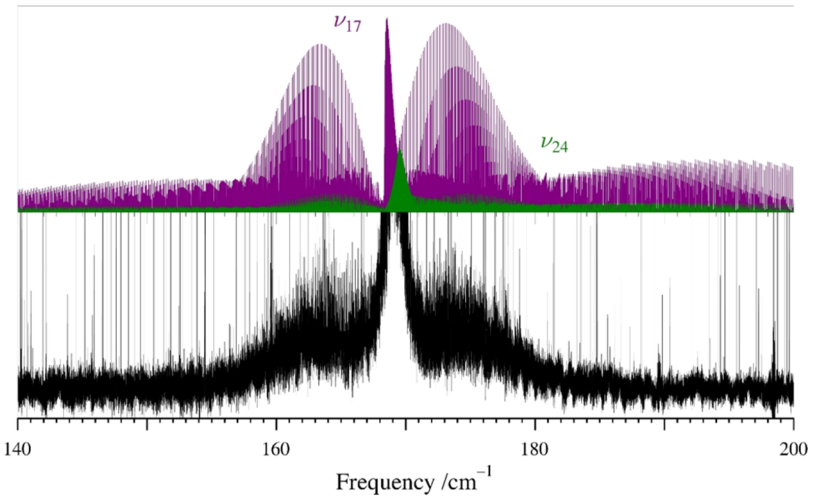

Figure 7. Predicted stick spectra (top) of ν_{17} (purple) and ν_{24} (green) of 3-furonitrile and the experimental high-resolution infrared spectrum (bottom).

each state. The quantum-number coverage is displayed in the data distribution plots of the rotational transitions in Figure 8 and of the infrared data in the Supporting Information. The maximum K_a'' analyzed was limited to 40 to avoid introducing unnecessary confusion or error due to the diminishingly low intensity of higher-K_a'' transitions and the potential for overlap with other transitions in an already quite extensive data set. Since ν_{17} and ν_{24} are quite close in energy, state-mixing is substantial at low K_a'', and the predominant coupling interactions are observed at K_a'' < 20. Thus, limiting the upper K_a'' range at 40 is not expected to significantly affect the determination of coupling parameters. Additionally, the transitions in the data set were drastically limited by the instability of rotational energy-level labels caused by the intense state-mixing. Although many series between $K_a \sim 4$ and 17 are readily visible in Loomis–Wood plots, and the frequencies are measurable within the experimental uncertainty, the state labels assigned to these frequencies change unpredictably between iterations of least-squares fitting, causing well-measured frequencies to be rejected and making convergence of the least-squares fit more difficult. In order to obtain a converged least-squares fit, many transitions with such unstable labels were excluded from the final data set. The resulting spectroscopic constants are provided in Table 2 alongside the ground-state constants from the least-squares fit without nuclear quadrupole coupling. In the end, Δ_K, Φ_{JK}, Φ_{KJ}, and the off-diagonal sextic terms of each vibrationally excited state could not be determined and were thus held constant at their corresponding ground-state values. The centrifugal distortion constants that could be determined are within 8% of the corresponding ground-state values, and none of these exhibit the equal-and-opposite magnitude of change that is characteristic of absorbed coupling. The only constants that do exhibit such behavior are the A_v constants. They are, however, both within 1% of the ground-state value, so if coupling was inappropriately absorbed into these constants, it seems to be fairly minimal (see discussion of vibration–rotation interaction

https://doi.org/10.1021/acs.jpca.4c03093
J. Phys. Chem. A XXXX, XXX, XXX–XXX

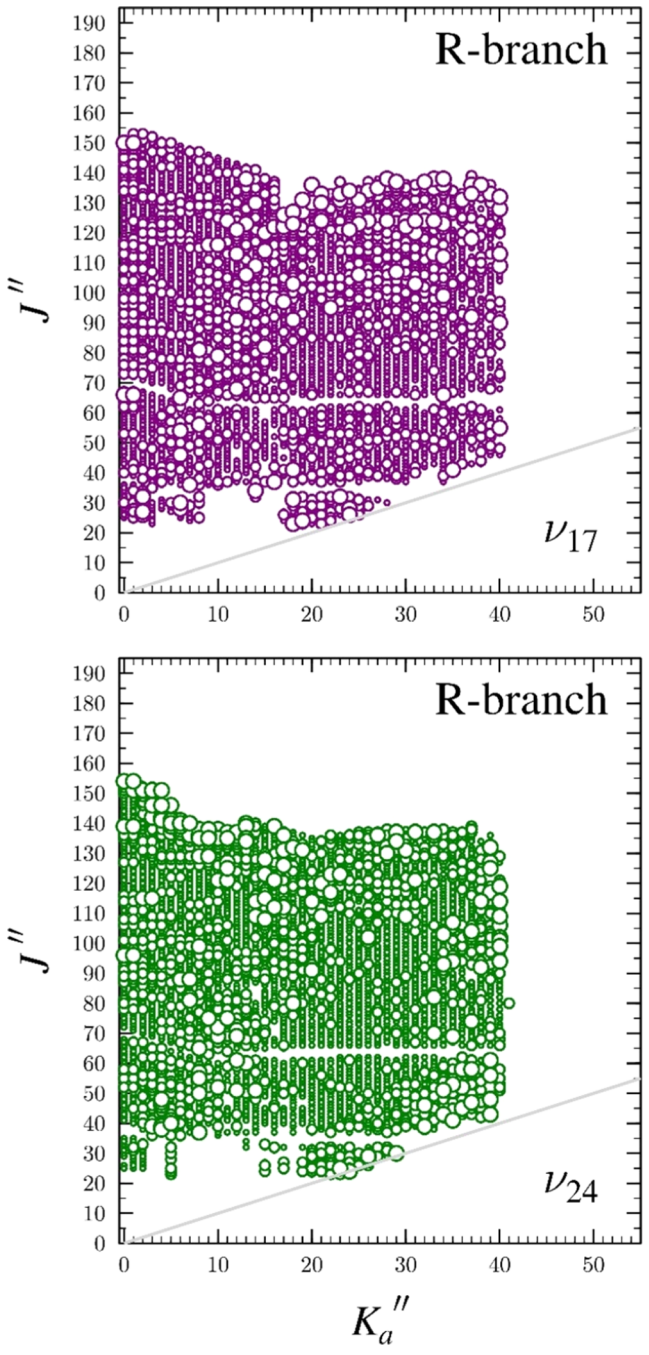

Figure 8. Data distribution plots for the least-squares fit of spectroscopic data for the pure rotational transitions of ν_{17} and ν_{24} of 3-furonitrile (data distribution plots for infrared transitions are provided in the Supporting Information). The size of the open circle is proportional to the value of $|(f_{obs.} - f_{calc.})/\delta f|$, where δf is the assumed frequency measurement uncertainty (50 kHz), and all of the quotient values are smaller than 3.

values, below). The other rotational constants are within 0.2% of the corresponding ground-state values. The vibrational energies are determined (ν_{17} = 168.193 164 8 (67) cm^{-1} and ν_{24} = 169.635 831 5 (77) cm^{-1}), and seven Coriolis-coupling terms (G_a, G_a^J, G_a^K, F_{bc}, F_{bc}^K, G_b, and F_{ac}) were needed to achieve a satisfactory least-squares fit.

The rotational constants provided in Table 2 for ν_{17} and ν_{24} were used to determine the vibration−rotation interaction constants $B_0 - B_v$ (Table 3). For both $B_0 - B_v$ and $C_0 - C_v$, the agreement between the theoretical values and the experimental values is as good as can be expected, all within 7, 6, or 1.5% for the values determined at the B3LYP, MP2, and CCSD(T) levels of theory, respectively. This agreement provides confidence in the quality of both the theoretical estimates and the experimental analysis. Given the small value of $|\zeta_{17,24}^b|$, it is not surprising that the agreement of the $B_0 - B_v$ values is comparable to the $C_0 - C_v$ values, indicating that the $B_0 - B_v$ values are not obviously perturbed by the Coriolis coupling. In contrast, the experimental and the CCSD(T) computed $A_0 - A_v$ values show the telltale effects of untreated Coriolis coupling: the $A_0 - A_{17}$ and $A_0 - A_{24}$ values have nearly equal, large magnitudes and opposite signs. The B3LYP and MP2 values calculated in Gaussian appear to be deperturbed and are significantly closer to the expected true $A_0 - A_v$ values. The combination of a quite large Coriolis-coupling coefficient (G_a = 15333.18 (30) MHz) and the very small energy separation between ν_{17} and ν_{24} ($\Delta E_{24,17}$ = 1.442 667 (10) cm^{-1}) results in an intensity of state-mixing that has rarely been described in the literature. It was, therefore, quite difficult to obtain completely unperturbed experimental $A_0 - A_v$ values. The computed energies of the two modes at the CCSD(T) level are in excellent agreement with their experimental values, each less than 1% deviation from the experimental values (0.5 and 1.4 cm^{-1} for ν_{17} and ν_{24}, respectively). The accuracies of the predictions are similarly close at the MP2 level of theory (0.3 and 1.8 cm^{-1} for ν_{17} and ν_{24}, respectively), but distinctly worse when predicted by B3LYP (9.3 and 5.9 cm^{-1} for ν_{17} and ν_{24}, respectively). Although the $\Delta E_{24,17}$ values have small *obs.* − *calc.* values (3.44, −1.46, and −0.86 cm^{-1} using B3LYP, MP2, and CCSD(T), respectively; see Table 3), the energy separation is predicted most accurately by CCSD(T). Unsuccessful attempts were made to find a set of *a*-axis Coriolis-coupling terms that provide more physically meaningful $A_0 - A_v$ values in the least-squares fitting with the current data set. This situation is not surprising for the reasons stated above and the inherent strong correlations between the A_v rotational constants and the *a*-axis Coriolis-coupling coefficients. Despite this limitation, the good agreement between experimental and predicted values for the averages of all of the vibration−rotation interaction constants (Table 3) provides confidence in the overall quality of the least-squares fit and its ability to provide a meaningful analysis of the Coriolis-coupled dyad.

The energy difference between the two fundamental states was well-determined from the coupling analysis using exclusively the rotational data, despite the fact that a satisfactory least-squares fit had not been obtained. At that stage, the fit was unable to consistently converge, and the quantum-number labels were not consistent between iterations. As shown in Figure 7, the infrared bands of ν_{17} and ν_{24} are sufficiently overlapped such that they are nearly indistinguishable. The initial assignment of the ν_{17} rotationally resolved infrared transitions was a one-parameter problem that necessitated visual alignment of the Q-branch and Loomis−Wood plots to confirm the assignments of individual R- and P-branch series. Neither fundamental state is particularly intense (5.2 and 2.4 km/mol for ν_{17} and ν_{24}, respectively, calculated by CCSD(T)), resulting in a relatively low signal-to-noise ratio in the high-resolution infrared spectrum. Without accurate predictions of the spectroscopic constants and the spectral pattern of the rotationally resolved transitions, the assignment of these transitions would have been quite difficult. Once a few of the ν_{17} infrared transitions were included in the data set, however, the ν_{24} transitions were

https://doi.org/10.1021/acs.jpca.4c03093
J. Phys. Chem. A XXXX, XXX, XXX−XXX

Table 2. Experimental Spectroscopic Constants for the Ground State and Vibrationally Excited States ν_{17} and ν_{24} of 3-Furonitrile (A-Reduced Hamiltonian, I^r Representation)

	ground state [a]	ν_{17} (A′, 168.7 cm^{-1}) [b,c]	ν_{24} (A″, 171.0 cm^{-1}) [b,c]
A_v (MHz)	9296.55253 (57)	9368.77 (21)	9224.77 (21)
B_v (MHz)	1940.269840 (35)	1944.875807 (92)	1943.263500 (96)
C_v (MHz)	1604.628513 (34)	1606.135425 (32)	1607.783143 (36)
Δ_J (kHz)	0.0728679 (34)	0.0748582 (14)	0.0745760 (13)
Δ_{JK} (kHz)	2.854516 (49)	2.93677 (19)	2.72608 (19)
Δ_K (kHz)	0.5153 (13)	[0.5153]	[0.5153]
δ_J (kHz)	0.0133908 (14)	0.01411807 (66)	0.01357977 (65)
δ_K (kHz)	1.62865 (12)	1.66846 (10)	1.623178 (98)
Φ_J (Hz)	−0.00000288 (21)	[−0.00000288]	[−0.00000288]
Φ_{JK} (Hz)	0.0066573 (64)	0.0066557 (72)	0.0065666 (70)
Φ_{KJ} (Hz)	−0.046046 (54)	−0.046513 (77)	−0.042725 (69)
Φ_K (Hz)	0.05096 (99)	[0.05096]	[0.05096]
ϕ_J (Hz)	0.000002384 (47)	[0.000002384]	[0.000002384]
ϕ_{JK} (Hz)	0.0031021 (51)	[0.0031021]	[0.0031021]
ϕ_K (Hz)	0.05430 (17)	[0.05430]	[0.05430]
Energy (MHz)		5042304.23 (20)	5085554.29 (23)
Energy (cm^{-1})		168.1931648 (67)	169.6358315 (77)
G_a (MHz)		15333.18 (30)	
G_a^J (MHz)		−0.021273 (26)	
G_a^K (MHz)		−0.1570 (10)	
F_{bc} (MHz)		1.2041 (22)	
F_{bc}^K (MHz)		0.00004355 (20)	
G_b (MHz)		−25.246 (85)	
F_{ac} (MHz)		−11.291 (13)	
Δ_i (uÅ^2) [d]	0.120389 (9)	0.8608 (12)	−0.5193 (12)
N_{lines} (rot) [e]	5655	4250	4345
N_{lines} (IR) [e]		728	150
σ_{fit} rot (MHz)	0.031	0.045	0.045
σ_{fit} IR (MHz)		5.17	6.01

[a]Ground-state (black) constants reproduced from Table 1 (this work only) for convenient comparison to those of ν_{17} (purple) and ν_{24} (green). [b]Fundamental frequency predicted using CCSD(T)/cc-pCVTZ. [c]Constants that could not be experimentally determined, including those not explicitly shown, were held constant at the corresponding ground-state value [in brackets] determined from the least-squares fit from this work only. [d]Inertial defect, $\Delta_i = I_c - I_a - I_b$, calculated using PLANM from the B_v constants. [e]Number of fitted transition frequencies.

Table 3. Vibration-Rotation Interaction and Coriolis-Coupling Constants of the ν_{17}-ν_{24} Dyad of 3-Furonitrile

	Experimental	B3LYP [a]	MP2 [a]	CCSD(T) [b]
$A_0 - A_{17}$ (MHz)	−72.22 (21)	−12.7	−13.0	2514.
$B_0 - B_{17}$ (MHz)	−4.60597 (10)	−4.38	−4.48	−4.55
$C_0 - C_{17}$ (MHz)	−1.506912 (47)	−1.41	−1.47	−1.50
$A_0 - A_{24}$ (MHz)	71.78 (21)	12.4	11.9	−2510.
$B_0 - B_{24}$ (MHz)	−2.99366 (10)	−2.94	−2.83	−2.97
$C_0 - C_{24}$ (MHz)	−3.154630 (47)	−3.08	−2.99	−3.11
$\frac{(A_0-A_{17})+(A_0-A_{24})}{2}$ (MHz)	−0.22 (30)	−0.165	−0.632	−0.411
$\frac{(B_0-B_{17})+(B_0-B_{24})}{2}$ (MHz)	−3.79981 (14)	−3.66	−3.66	−3.76
$\frac{(C_0-C_{17})+(C_0-C_{24})}{2}$ (MHz)	−2.330771 (68)	−2.24	−2.23	−2.30
$\lvert\zeta^a_{17,24}\rvert$	0.82467	0.81699	0.82185	0.82044
$\lvert\zeta^b_{17,24}\rvert$	0.00651	0.00169	0.00580	0.00522
E_{17} (cm^{-1})	168.1931648 (67)	177.5	168.5	168.7
E_{24} (cm^{-1})	169.6358315 (77)	175.5	171.4	171.0
$\Delta E_{24,17}$ (cm^{-1})	1.442667 (10)	−2.0	2.9	2.3

[a]Evaluated with the 6-311+G(2d,p) basis set. [b]Evaluated with the cc-pCVTZ basis set.

predicted within their nominal experimental uncertainty and easy to assign, despite the low intensity, low signal-to-noise ratio, and the overlap of the ν_{24} and ν_{17} spectra. Given the complexity of the coupling analysis, an independent measurement of the vibrational energies from the high-resolution infrared spectrum was quite helpful.

https://doi.org/10.1021/acs.jpca.4c03093
J. Phys. Chem. A XXXX, XXX, XXX−XXX

The least-squares fitting of this dyad was particularly challenging in comparison to the other cyanoarene dyads that have been studied recently by our group. As previously mentioned, the combination of the large values of A_0 and $|\zeta^a_{17,24}|$ for 3-furonitrile gives rise to a large G_a constant. The very small energy separation between the two vibrationally excited states leads to intense state-mixing, even at relatively low values of J and K compared to the other cyanoarenes.[22−29] None of the available diagonalization options in SPFIT led to a stable set of quantum numbers. Between iterations, many of the measured transitions changed quantum-number assignments, causing SPFIT to reject these transitions. For a coupled-dyad system, this behavior presents a substantial limitation, as the transitions that are prone to quantum-number changes include those that are heavily state-mixed. It is precisely these transitions that are important in determining the coupling constants and reducing the correlations between coupling, rotational, and centrifugal distortion constants. A similar occurrence has been described for propionitrile,[44] where the transitions with unstable quantum numbers were assigned very large nominal uncertainties, effectively removing them from the least-squares fit. To obtain a stable fit that produced stable constants, we employed an analogous technique and excluded transitions with unstable quantum-number labels from the data set. An artifact of this intense state-mixing can be seen in Figure 9. The ν_{24} $K_a = 14^+$ and ν_{24} $K_a = 14^-$ series form a smooth curve in the bottom series of transitions. Many transitions along this curve, and the analogous ones for other K_a series, were able to be included in the data set when the quantum-number labels of their energy levels remained constant. In other coupled dyads of cyanoarenes, where the mixing was less intense, these transitions represent a single K_a series from one vibrational state.

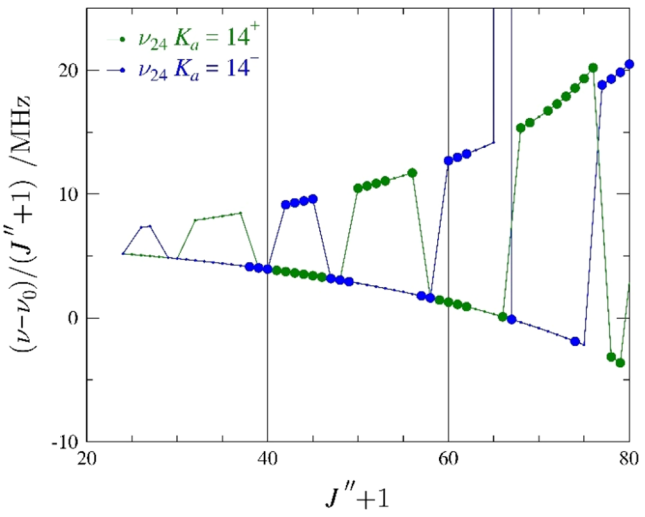

Figure 9. K_a series plots for 3-furonitrile showing the $K_a = 14^+$ series (green) for ν_{24} and the $K_a = 14^-$ series (blue) for ν_{24}. There are no transitions for which the *obs.* − *calc.* value exceeds 150 kHz or 3 times the nominal experimental uncertainty. The plotted values are frequency differences between excited-state transitions and their ground-state counterparts $(\nu - \nu_0)$, scaled by $(J'' + 1)$ in order to make the plots more horizontal.

The typical resonance progression plots (Figure 10) that we employ show the progression of the Coriolis-coupling-induced resonances along K_a series. For the 3-furonitrile data set, where the quantum-number labels are not static in SPFIT/SPCAT,

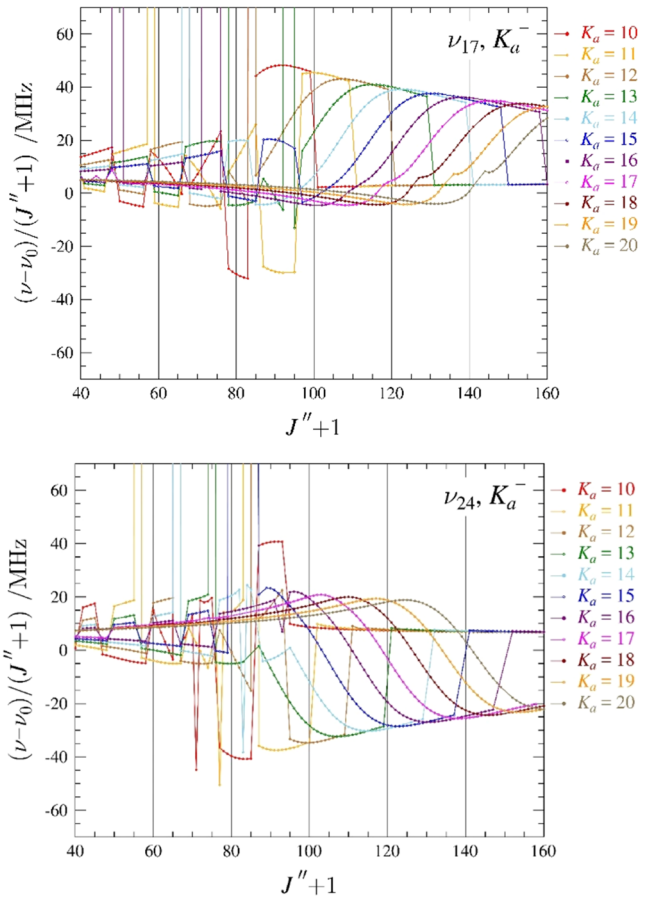

Figure 10. Superimposed resonance plots of ν_{17} (upper) $^aR_{0,1}$ K_a^- series ν_{24} (lower) $^aR_{0,1}$ K_a^- series from 10 to 20 for 3-furonitrile. Measured transitions are omitted for clarity, but those that are included in the data set are indistinguishable from the plotted values on this scale. The plotted values are frequency differences between excited-state transitions and their ground-state counterparts $(\nu - \nu_0)$, scaled by $(J'' + 1)$.

these plots reveal more complex behavior. At much higher values of J, the K_a series experiences sharp discontinuities that have matching behavior with $\Delta K_a = 1$ selection rules. For example, the $K_a = 14^+/15^-$ degenerate series of ν_{24} and the $K_a = 14^+/13^-$ degenerate series of ν_{17} both display smooth series with a sharp increase or decrease in $(\nu - \nu_0)/(J'' + 1)$ between $J'' + 1 = 136$ and 141, which results in a new, smooth series as J increases. Analogous discontinuities exist in all of the nearby K_a series, and as K_a increases, these discontinuities progress to higher values of J. Transitions before and after the discontinuities were included in the least-squares fit. A few resonances are discernible in this plot, although the resonant transitions that correspond to those resonances were not included in the final data set due to quantum-number instability and not due to the inability of the spectroscopic constants to model and predict a transition at that frequency.

As a result of the quantum-number instability, it is nearly impossible to do the analysis of resonant transitions or nominal interstate transitions using SPFIT/SPCAT that we employed in analogous works. Despite this limitation, we are confident in the quality of the B_v and C_v rotational and centrifugal distortion constants obtained from the least-squares fit; they are likely to be physically meaningful. The A_v values should be viewed as effective constants. The Coriolis-coupling parameters, com-

https://doi.org/10.1021/acs.jpca.4c03093
J. Phys. Chem. A XXXX, XXX, XXX−XXX

Table 4. Energy Differences between In-Plane (ip) and Out-of-Plane (oop) Nitrile Bending Modes for Cyanoarenes

	out-of-plane	in-plane	ΔE_{ip-oop} (cm^{-1})	A_0	$\lvert\zeta^a_{x,y}\rvert$
benzonitrile[22,25]	ν_{22}, B_1	ν_{33}, B_2	19.108 170 1 (74)	5655.265 371 (75)	0.841
2-cyanopyridine[28]	ν_{30}, A″	ν_{21}, A′	26.524 312 6 (40)	5837.001 016 (84)	0.848
3-cyanopyridine[24]	ν_{30}, A″	ν_{21}, A′	15.752 469 3 (37)	5823.058 32 (11)	0.833
4-cyanopyridine[23]	ν_{20}, B_1	ν_{30}, B_2	18.806 554 (11)	6000.670 28 (91)	0.843
2-cyanopyrimidine[27]	ν_{18}, B_1	ν_{27}, B_2	38.967 319 1 (77)	6043.453 9 (12)	0.873
cyanopyrazine[26]	ν_{27}, A″	ν_{19}, A′	24.824 596 2 (60)	6003.129 84 (58)	0.899
2-furonitrile[29]	ν_{24}, A″	ν_{17}, A′	11.779 103 9 (36)	9220.251 42 (10)	0.806
3-furonitrile	**ν_{24}, A″**	**ν_{17}, A′**	−1.442 667 (10)	9296.552 53 (57)	**0.825**

bined with the other spectroscopic constants, accurately model the observed spectra and determine the vibrational energies. The physical meaning of the Coriolis-coupling values determined in the least-squares fit is ambiguous. These values should be viewed as potentially effective. Prior to obtaining the high-resolution infrared spectra, the initial least-squares fit of the millimeter-wave data set determined an accurate and precise $\Delta E_{24,17}$ value. The accuracy of this value became clear when the initial assignment of the infrared spectrum of ν_{17} resulted in the immediate, accurate prediction of ν_{24} infrared transitions. When the predicted spectrum was aligned with the experimental spectrum of ν_{17} using Loomis−Wood plots and several infrared transitions were incorporated into the data set, the least-squares fit produced spectroscopic constants that predicted the spectrum of ν_{24} within experimental error. Such an accurate prediction allowed ν_{24} transitions to be assigned, measured, and least-squares fit with relative ease. In the end, the spectroscopic constants and $\Delta E_{24,17}$ value adequately model the rotational and infrared spectra of each state, a feat that would not be possible without the accurate and precise determination of the energies of each vibrational state and overall treatment of the coupling interaction.

In all cases of cyanoarenes with six-membered rings previously studied (Table 4), the out-of-plane bending frequencies are lower in energy than the in-plane modes by 15−39 cm^{-1}. Of the previously studied cyanoarenes, 2-furonitrile had the smallest energy separation of 11.8 cm^{-1} between these two fundamental states. In interesting contrast to the other cyanoarenes in Table 4, 3-furonitrile is the only case with the in-plane (ip) vibration (ν_{17}) lower in energy than the out-of-plane (oop) vibration (ν_{24}), ΔE_{ip-oop} = −1.442 667 (10) cm^{-1}. This energy separation was determined from both the inclusion of high-resolution infrared data for both modes and the coupling analysis. The physical origin of the change in ΔE_{ip-oop} between 2- and 3-furonitrile by ∼13 cm^{-1} is unclear. A difference of similar magnitude (∼11 cm^{-1}) was observed for 2- and 3-cyanopyridine, with the larger energy gap between the modes occurring when the nitrile group was attached to the carbon adjacent to the heteroatom.

Reanalysis of the Ground Vibrational State of 2-Furonitrile. As described above, two contemporaneous works (by our group[29] and Melosso *et al.*[13]) provided complementary analyses of the rotational spectra of 2-furonitrile. In the current study, we combined all available rotational transitions and high-resolution infrared transitions (including two works inadvertently overlooked in our previous investigation)[11,30] and fit these data to obtain a refined set of spectroscopic constants (Table 5). For comparison, Table 5 also includes the constants from our original least-squares fit that does not include microwave transitions or those with resolved nuclear hyperfine coupling. The reanalysis of the data set for 2-furonitrile provides the best available experimental spectroscopic constants for prediction of the rotational transitions outside the currently observed frequency range. The changes in the spectroscopic constants between the two data sets for 2-furonitrile also provide insight into the differences between the two analogous data sets for 3-furonitrile (Table 1). As described above, the computed and experimental h_1 and ϕ_J constants determined from transitions <320 GHz[13] for 3-furonitrile agree more closely with one another than with those obtained using the data set up to 500 GHz. As we suggested earlier, the poorer agreement when using a higher-frequency range is due to untreated, higher-order centrifugal distortion influencing those constants for 3-furonitrile. Supporting this assumption, a similar deviation between the computed and experimental h_1 constants is observed for 2-furonitrile. The experimental value of h_1 for 2-furonitrile is about half the size of its computed value when rotational transitions up to 750 GHz are included, but is in close agreement with its computed value when the data set is limited to 320 GHz in the previous work.[13] Parallel behavior is observed for the Φ_J and ϕ_J spectroscopic constants between 2- and 3-furonitrile. When the data set is limited to <320 GHz, the computed and experimental values of the spectroscopic constants are in close agreement, but show similar deviations when higher-frequency transitions are included. A satisfactory least-squares fit of 2-furonitrile up to 750 GHz requires additional octic centrifugal distortion constants in the Hamiltonian model compared to 3-furonitrile, which supports the argument that (as expected) the higher-frequency data requires more centrifugal distortion terms and that an incomplete treatment of the centrifugal distortion can impact the fitted spectroscopic terms in unphysical ways.

CONCLUSIONS

By combining the previously available data with new frequency measurements, this study provides the best available data to conduct astronomical searches for 2-furonitrile or 3-furonitrile across the frequency range of available radiotelescopes. The least-squares fitting of the Coriolis-coupled dyad (ν_{17} and ν_{24}) for 3-furonitrile was challenging as a result of the very small energy separation and the very strong coupling interaction, as manifest by the large value of Coriolis-coupling term G_a. Even with well-determined spectroscopic constants from the ground vibrational state, the least-squares fitting was made especially difficult by the instability of quantum-number labels between iterations of the least-squares fitting. While we addressed this problem by excluding the transitions that are prone to quantum-number changes due to substantial state-mixing, alternative solutions are possible that address this issue in a more sophisticated way. One could implement a quantum-number labeling method based upon the largest magnitude eigenvector-squared after diagonalization. Alternatively, one could imple-

https://doi.org/10.1021/acs.jpca.4c03093
J. Phys. Chem. A XXXX, XXX, XXX−XXX

Table 5. Experimental and Computational Spectroscopic Constants for the Ground Vibrational State of 2-Furonitrile (S- and A-Reduced Hamiltonian, I^r Representation)

	S reduction, I^r representation				A reduction, I^r representation		
	experimental (ref 29)[a]	experimental (combined)[a,b]	CCSD(T)[c]		experimental (ref 29)[a]	experimental (combined)[a,b]	CCSD(T)[c]
A_0 (MHz)	9220.25142 (10)	9220.251375 (71)	9173	A_0 (MHz)	9220.25121 (10)	9220.251217 (71)	9173
B_0 (MHz)	2029.274136 (17)	2029.274038 (13)	2020	B_0 (MHz)	2029.277357 (17)	2029.277268 (13)	2020
C_0 (MHz)	1662.643524 (17)	1662.643425 (13)	1655	C_0 (MHz)	1662.640345 (17)	1662.640245 (13)	1655
D_J (kHz)	0.0596802 (19)	0.0596622 (15)	0.0568	Δ_J (kHz)	0.0796708 (19)	0.0796535 (16)	0.0762
D_{JK} (kHz)	2.910358 (21)	2.910318 (19)	2.89	Δ_{JK} (kHz)	2.790339 (21)	2.790303 (19)	2.89
D_K (kHz)	0.29747 (20)	0.29773 (15)	0.237	Δ_K (kHz)	0.39739 (20)	0.39771 (15)	0.218
d_1 (kHz)	−0.01517569 (50)	−0.01517572 (42)	−0.0144	δ_J (kHz)	0.01517638 (53)	0.01517663 (44)	0.0144
d_2 (kHz)	−0.00999786 (30)	−0.00999813 (30)	−0.00966	δ_K (kHz)	1.608947 (46)	1.609004 (46)	1.63
H_J (Hz)	−0.000028009 (84)	−0.000028825 (71)	−0.00003220	Φ_J (Hz)	0.000009193 (91)	0.000008431 (78)	0.00000390
H_{JK} (Hz)	0.0045065 (17)	0.0044995 (16)	0.00441	Φ_{JK} (Hz)	0.0066278 (65)	0.0066300 (65)	0.00645
H_{KJ} (Hz)	−0.035910 (15)	−0.035900 (14)	−0.0363	Φ_{KJ} (Hz)	−0.043606 (26)	−0.043625 (26)	−0.0436
H_K (Hz)	0.03381 (16)	0.03398 (14)	0.0334	Φ_K (Hz)	0.03931 (16)	0.03955 (14)	0.0387
h_1 (Hz)	−0.000000851 (15)	−0.000000852 (13)	−0.00000180	ϕ_J (Hz)	0.000002606 (17)	0.000002606 (15)	0.00000170
h_2 (Hz)	0.000018831 (30)	0.000018872 (30)	0.000010	ϕ_{JK} (Hz)	0.0033275 (43)	0.0033341 (43)	0.00325
h_3 (Hz)	0.000003719 (13)	0.000003730 (13)	0.00000350	ϕ_K (Hz)	0.04928 (17)	0.04952 (17)	0.04786
L_J (mHz)	0.0000000173 (13)	0.0000000287 (11)		L_J (mHz)	−0.0000000358 (15)	−0.0000000258 (14)	
L_{JJK} (mHz)	−0.000011414 (32)	−0.000011272 (32)		L_{JJK} (mHz)	−0.00001420 (18)	−0.00001444 (18)	
L_{JK} (mHz)	0.00015018 (50)	0.00015105 (50)		L_{JK} (mHz)	0.00011551 (72)	0.00011747 (71)	
L_{KKJ} (mHz)	−0.0015285 (40)	−0.0015332 (39)		L_{KKJ} (mHz)	−0.0013964 (40)	−0.0014021 (38)	
L_K (mHz)	0.001142 (44)	0.001103 (38)		L_K (mHz)	0.001052 (44)	0.001003 (38)	
l_1 (mHz)	[0.]	[0.]		l_J (mHz)	[0.]	[0.]	
l_2 (mHz)	−0.00000003136 (69)	−0.00000003265 (69)		l_{JK} (mHz)	−0.000006118 (94)	−0.000006293 (95)	
l_3 (mHz)	−0.00000000698 (45)	−0.00000000758 (46)		l_{KJ} (mHz)	−0.0000363 (49)	−0.0000468 (50)	
l_4 (mHz)	−0.00000000161 (12)	−0.00000000173 (13)		l_K (mHz)	[0.]	[0.]	
$3/2\ \chi_{aa}$ (MHz)		−6.4408 (12)	−6.434[d]			−6.4409 (12)	−6.434[d]
$(\chi_{bb} - \chi_{cc})/4$ (MHz)		0.25704 (37)	0.269[d]			0.25693 (38)	0.269[d]
Δ_i (uÅ^2)[e]	0.105059 (4)	0.105065 (3)	0.083141		0.106034 (4)	0.106041 (3)	0.083141
N_{lines}[f]	10143	10309			10143	10309	
σ_{fit} (MHz)	0.040	0.040			0.040	0.040	

[a]Parameters in brackets were held constant at zero. [b]Includes transitions from refs 11,13,29,30. [c]Evaluated with the cc-pCVTZ basis set. [d]Value from ref 13. [e]Inertial defect, $\Delta_i = I_c - I_a - I_b$, calculated using PLANM from the B_0 constants. [f]Number of fitted transition frequencies.

https://doi.org/10.1021/acs.jpca.4c03093
J. Phys. Chem. A XXXX, XXX, XXX−XXX

ment a least-squares fitting routine that allows the quantum-number labels to be revised in each iteration to values that most closely match the energy levels or transition frequencies. Such a fitting routine would allow the spectroscopic constants to model the rotational energy levels in a manner independent of the quantum-number labels, which might change for a particular energy level as the state-mixing changes in the least-squares fitting process. Either of these approaches to a least-squares fitting routine would offer significant advantages in cases such as 3-furonitrile by allowing more measurable transitions to be included in the least-squares fit.

There are two potential tests to determine whether important centrifugal distortion is being improperly modeled for both furonitriles and to resolve the differences in the sextic centrifugal distortion constants between the computed values, previous work, and the combined data sets presented here. First, it has long been a common practice to hold important centrifugal distortion constants fixed at an estimated value (to the corresponding value of a different vibrational state, to the corresponding value of a different isotopologue, to a computed value, *etc.*) if these constants cannot be adequately determined in least-squares fitting. Such a practice prevents their exclusion from impacting the values of other parameters that are being fit. While it is unlikely that appropriate experimental values will be available to use in these least-squares fits, it may be possible in the future to hold the excluded octic centrifugal distortion constants at their computed values. The computed values of the unfit octic terms should bring the sextic constants into better agreement with the computed values if they can account for currently untreated centrifugal distortion. Alternatively, the data sets for 2- and 3-furonitrile could be expanded by measuring higher-frequency transitions with even higher J and K quantum numbers. A sufficiently expanded data set would provide more spectroscopic information about the octic centrifugal distortion, making it possible to adequately determine a complete set of octic constants and provide a better determination of the sextic constants as a result. Even with over 10,000 independent transitions with frequencies up to 750 GHz, however, the spectroscopic data is insufficient to determine a complete set of octic constants for 2-furonitrile. It is therefore likely that, even with a better signal-to-noise ratio in the 500−750 GHz frequency region, the addition of this data would not be sufficient to determine all of the octic centrifugal distortion constants for 3-furonitrile, either. Expanding the data set sufficiently to provide enough spectroscopic information to determine all of the octic centrifugal distortion constants therefore represents a significant challenge. In the meantime, the experimental sextic centrifugal distortion constants should be considered at least slightly empirical and the computed values of h_1, Φ_J, and ϕ_J should be regarded as more physically meaningful than the values determined experimentally in this work.

■ ASSOCIATED CONTENT

Supporting Information

The Supporting Information is available free of charge at https://pubs.acs.org/doi/10.1021/acs.jpca.4c03093.

Computational output files and least-squares fitting files for all vibrational states (ZIP)

Data set distribution plots of IR data for ν_{24} and ν_{17} (PDF)

■ AUTHOR INFORMATION

Corresponding Authors

Robert J. McMahon − *Department of Chemistry, University of Wisconsin−Madison, Madison, Wisconsin 53706, United States;* orcid.org/0000-0003-1377-5107; Email: robert.mcmahon@wisc.edu

R. Claude Woods − *Department of Chemistry, University of Wisconsin−Madison, Madison, Wisconsin 53706, United States;* orcid.org/0000-0003-0865-4693; Email: rcwoods@wisc.edu

Authors

William H. Styers − *Department of Chemistry, University of Wisconsin−Madison, Madison, Wisconsin 53706, United States*

Maria A. Zdanovskaia − *Department of Chemistry, University of Wisconsin−Madison, Madison, Wisconsin 53706, United States;* orcid.org/0000-0001-5167-8573

Brian J. Esselman − *Department of Chemistry, University of Wisconsin−Madison, Madison, Wisconsin 53706, United States;* orcid.org/0000-0002-9385-8078

Andrew N. Owen − *Department of Chemistry, University of Wisconsin−Madison, Madison, Wisconsin 53706, United States;* orcid.org/0000-0001-5903-1651

Samuel M. Kougias − *Department of Chemistry, University of Wisconsin−Madison, Madison, Wisconsin 53706, United States;* orcid.org/0000-0002-9877-0817

Brant E. Billinghurst − *Canadian Light Source Inc., University of Saskatchewan, Saskatoon, Saskatchewan S7N 2V3, Canada*

Jianbao Zhao − *Canadian Light Source Inc., University of Saskatchewan, Saskatoon, Saskatchewan S7N 2V3, Canada;* orcid.org/0000-0003-3864-2167

Complete contact information is available at: https://pubs.acs.org/10.1021/acs.jpca.4c03093

Notes

The authors declare no competing financial interest.

■ ACKNOWLEDGMENTS

We gratefully acknowledge funding from the U.S. National Science Foundation for support of this project (CHE-2245738 and CHE-1954270). We thank Michael McCarthy for the loan of an amplification−multiplication chain. Part of the research described in this paper was performed at the Canadian Light Source, a national research facility of the University of Saskatchewan, which is supported by the Canada Foundation for Innovation (CFI), the Natural Sciences and Engineering Research Council (NSERC), the National Research Council (NRC), the Canadian Institutes of Health Research (CIHR), the Government of Saskatchewan, and the University of Saskatchewan.

■ REFERENCES

(1) Simon, M. N.; Simon, M. Search for Interstellar Acrylonitrile, Pyrimidine, and Pyridine. *Astrophys. J.* **1973**, *184*, 757−761.

(2) Kuan, Y.-J.; Yan, C.-H.; Charnley, S. B.; Kisiel, Z.; Ehrenfreund, P.; Huang, H.-C. A Search for Interstellar Pyrimidine. *Mon. Not. R. Astron. Soc.* **2003**, *345*, 650−656.

(3) Charnley, S. B.; Kuan, Y.-J.; Huang, H.-C.; Botta, O.; Butner, H. M.; Cox, N.; Despois, D.; Ehrenfreund, P.; Kisiel, Z.; Lee, Y.-Y.; et al. Astronomical Searches for Nitrogen Heterocycles. *Adv. Space Res.* **2005**, *36*, 137−145.

(4) Lattelais, M.; Ellinger, Y.; Matrane, A.; Guillemin, J.-C. Looking for Heteroaromatic Rings and Related Isomers as Interstellar Candidates. *Phys. Chem. Chem. Phys.* **2010**, *12*, 4165−4171.
(5) Etim, E. E.; Adelagun, R. O. A.; Andrew, C.; Oluwole, O. E. Optimizing the Searches for Interstellar Heterocycles. *Adv. Space Res.* **2021**, *68*, 3508−3520.
(6) Dezafra, R. L.; Thaddeus, P.; Kutner, M.; Scoville, N.; Solomon, P. M.; Weaver, H.; Williams, D. R. W. Search for Interstellar Furan and Imidazole. *Astrophys. Lett.* **1972**, *10*, 1.
(7) Kutner, M. L.; Machnik, D. E.; Tucker, K. D.; Dickman, R. L. Search for Interstellar Pyrrole and Furan. *Astrophys. J.* **1980**, *242*, 541−544.
(8) McGuire, B. A.; Burkhardt, A. M.; Kalenskii, S. V.; Shingledecker, C. N.; Remijan, A. J.; Herbst, E.; McCarthy, M. C. Detection of the Aromatic Molecule Benzonitrile (*c*-C_6H_5CN) in the Interstellar Medium. *Science* **2018**, *359*, 202−205.
(9) Barnum, T. J.; Siebert, M. A.; Lee, K. L. K.; Loomis, R. A.; Changala, P. B.; Charnley, S. B.; Sita, M. L.; Xue, C.; Remijan, A. J.; Burkhardt, A. M.; et al. A Search for Heterocycles in GOTHAM Observations of TMC-1. *J. Phys. Chem. A* **2022**, *126*, 2716−2728.
(10) Oh, J. J.; Hillig, K. W.; Kuczkowski, R. L.; Bohn, R. K. Dipole Moments of Furan-Argon and Pyrrole-Argon. *J. Phys. Chem. A* **1990**, *94*, 4453−4455.
(11) Kojima, T.; Ogata, T.; Maeda, S. Microwave Spectrum of 2-Furancarbonitrile. *Chem. Lett.* **1976**, *5*, 607−610.
(12) Wiese, J.; Engelbrecht, L.; Dreizler, H. Improved Rotational Constants and Dipole Moment and a Nuclear Quadrupole Coupling Analysis of 2-Cyanothiophene and Dipole Moment of 2-Cyanofurane. *Z. Naturforsch., A* **1977**, *32*, 152−155.
(13) Melosso, M.; Alessandrini, S.; Spada, L.; Melli, A.; Wang, X.; Zheng, Y.; Duan, C.; Li, J.; Du, W.; Gou, Q.; et al. Rotational Spectra and Semi-Experimental structures of Furonitrile and its Water Cluster. *Phys. Chem. Chem. Phys.* **2023**, *25*, 31281−31291.
(14) Simbizi, R.; Nduwimana, D.; Niyoncuti, J.; Cishahayo, P.; Gahungu, G. On the Formation of 2- and 3-Cyanofurans and Their Protonated Forms in Interstellar Medium Conditions: Quantum Chemical Evidence. *RSC Adv.* **2022**, *12*, 25332−25341.
(15) McGuire, B. A.; Loomis, R. A.; Burkhardt, A. M.; Lee, K. L. K.; Shingledecker, C. N.; Charnley, S. B.; Cooke, I. R.; Cordiner, M. A.; Herbst, E.; Kalenskii, S.; et al. Detection of Two Interstellar Polycyclic Aromatic Hydrocarbons via Spectral Matched Filtering. *Science* **2021**, *371*, 1265−1269.
(16) Sita, M. L.; Changala, P. B.; Xue, C.; Burkhardt, A. M.; Shingledecker, C. N.; Lee, K. L. K.; Loomis, R. A.; Momjian, E.; Siebert, M. A.; Gupta, D.; et al. Discovery of Interstellar 2-Cyanoindene (2-C_9H_7CN) in GOTHAM Observations of TMC-1. *Astrophys. J. Lett.* **2022**, *938*, L12.
(17) McNaughton, D.; Jahn, M. K.; Travers, M. J.; Wachsmuth, D.; Godfrey, P. D.; Grabow, J.-U. Laboratory Rotational Spectroscopy of Cyano Substituted Polycyclic Aromatic Hydrocarbons. *Mon. Not. R. Astron. Soc.* **2018**, *476*, 5268−5273.
(18) Vogt, N.; Nair, K. P. R.; Grabow, J.-U.; Demaison, J. Microwave Rotational Spectrum and ab initio Computations on 4-Cyanopyridine: Molecular Structure and Hyperfine Interactions. *Mol. Phys.* **2018**, *116*, 3530−3537.
(19) Vogt, N.; Khaikin, L. S.; Rykov, A. N.; Grikina, O. E.; Batiukov, A. A.; Vogt, J.; Kochikov, I. V.; Shishkov, I. F. The Equilibrium Molecular Structure of 2-Cyanopyridine from Combined Analysis of Gas-phase Electron Diffraction and Microwave Data and Results of *ab initio* Calculations. *Struct. Chem.* **2019**, *30*, 1699−1706.
(20) Chitarra, O.; Lee, K. L. K.; Buchanan, Z.; Melosso, M.; McGuire, B. A.; Goubet, M.; Pirali, O.; Martin-Drumel, M.-A. Hunting the Relatives of Benzonitrile: Rotational Spectroscopy of Dicyanobenzenes. *Astron. Astrophys.* **2021**, *652*, A163.
(21) Buchanan, Z.; Lee, K. L. K.; Chitarra, O.; McCarthy, M. C.; Pirali, O.; Martin-Drumel, M.-A. A Rotational and Vibrational Investigation of Phenylpropiolonitrile ($C_6H_5C_3N$). *J. Mol. Spectrosc.* **2021**, *377*, No. 111425.
(22) Zdanovskaia, M. A.; Esselman, B. J.; Lau, H. S.; Bates, D. M.; Woods, R. C.; McMahon, R. J.; Kisiel, Z. The 103−360 GHz Rotational Spectrum of Benzonitrile, the First Interstellar Benzene Derivative Detected by Radioastronomy. *J. Mol. Spectrosc.* **2018**, *351*, 39−48.
(23) Dorman, P. M.; Esselman, B. J.; Park, J. E.; Woods, R. C.; McMahon, R. J. Millimeter-Wave Spectrum of 4-Cyanopyridine in its Ground state and Lowest-Energy Vibrationally Excited States, ν_{20} and ν_{30}. *J. Mol. Spectrosc.* **2020**, *369*, No. 111274.
(24) Dorman, P. M.; Esselman, B. J.; Woods, R. C.; McMahon, R. J. An Analysis of the Rotational Ground State and Lowest-Energy Vibrationally Excited Dyad of 3-Cyanopyridine: Low Symmetry Reveals Rich Complexity of Perturbations, Couplings, and Interstate Transitions. *J. Mol. Spectrosc.* **2020**, *373*, No. 111373.
(25) Zdanovskaia, M. A.; Martin-Drumel, M.-A.; Kisiel, Z.; Pirali, O.; Esselman, B. J.; Woods, R. C.; McMahon, R. J. The Eight Lowest-Energy Vibrational States of Benzonitrile: Analysis of Coriolis and Darling-Dennison Couplings by Millimeter-Wave and Far-Infrared Spectroscopy. *J. Mol. Spectrosc.* **2022**, *383*, No. 111568.
(26) Esselman, B. J.; Zdanovskaia, M. A.; Smith, H. H.; Woods, R. C.; McMahon, R. J. The 130−500 GHz Rotational Spectroscopy of Cyanopyrazine ($C_4H_3N_2$-CN). *J. Mol. Spectrosc.* **2022**, *389*, No. 111703.
(27) Smith, H. H.; Esselman, B. J.; Zdanovskaia, M. A.; Woods, R. C.; McMahon, R. J. The 130−500 GHz Rotational Spectrum of 2-Cyanopyrimidine. *J. Mol. Spectrosc.* **2023**, *391*, No. 111737.
(28) Dorman, P. M.; Esselman, B. J.; Zdanovskaia, M. A.; Woods, R. C.; McMahon, R. J. The 130 − 750 GHz Rotational Spectrum of 2-Cyanopyridine − Analysis of the Ground Vibrational State and the Coriolis-Coupled Dyad of its Lowest-Energy Fundamental States. *J. Mol. Spectrosc.* **2023**, *398*, No. 111842.
(29) Esselman, B. J.; Zdanovskaia, M. A.; Styers, W. H.; Owen, A. N.; Kougias, S. M.; Billinghurst, B. E.; Zhao, J.; Woods, R. C.; McMahon, R. J. Millimeter-Wave and High-Resolution Infrared Spectroscopy of 2-Furonitrile—A Highly Polar Substituted Furan. *J. Phys. Chem. A* **2023**, *127*, 1909−1922.
(30) Engelbrecht, L.; Sutter, D. H. Microwave Spectrum, Partial r_0-Structure and ^{14}N-Quadrupole Coupling Constants of 2-Cyanfurane. *Z. Naturforsch. A* **1976**, *31*, 670−672.
(31) Amberger, B. K.; Esselman, B. J.; Stanton, J. F.; Woods, R. C.; McMahon, R. J. Precise Equilibrium Structure Determination of Hydrazoic Acid (HN_3) by Millimeter-wave Spectroscopy. *J. Chem. Phys.* **2015**, *143*, No. 104310.
(32) Esselman, B. J.; Amberger, B. K.; Shutter, J. D.; Daane, M. A.; Stanton, J. F.; Woods, R. C.; McMahon, R. J. Rotational Spectroscopy of Pyridazine and its Isotopologs from 235−360 GHz: Equilibrium Structure and Vibrational Satellites. *J. Chem. Phys.* **2013**, *139*, No. 224304.
(33) Kisiel, Z.; Pszczółkowski, L.; Drouin, B. J.; Brauer, C. S.; Yu, S.; Pearson, J. C.; Medvedev, I. R.; Fortman, S.; Neese, C. Broadband Rotational Spectroscopy of Acrylonitrile: Vibrational Energies from Perturbations. *J. Mol. Spectrosc.* **2012**, *280*, 134−144.
(34) Kisiel, Z.; Pszczółkowski, L.; Medvedev, I. R.; Winnewisser, M.; De Lucia, F. C.; Herbst, E. Rotational Spectrum of *Trans*−*Trans* Diethyl Ether in the Ground and Three Excited Vibrational States. *J. Mol. Spectrosc.* **2005**, *233*, 231−243.
(35) Pickett, H. M. The Fitting and Prediction of Vibration-Rotation Spectra with Spin Interactions. *J. Mol. Spectrosc.* **1991**, *148*, 371−377.
(36) Kisiel, Z. PROSPE - Programs for ROtational SPEctroscopy. http://info.ifpan.edu.pl/~kisiel/prospe.htm (accessed Jan 2023).
(37) Frisch, M. J.; Trucks, G. W.; Schlegel, H. B.; Scuseria, G. E.; Robb, M. A.; Cheeseman, J. R.; Scalmani, G.; Barone, V.; Petersson, G. A.; Nakatsuji, H.et al. *Gaussian 16*, Revision C.01, Gaussian, Inc.: Wallingford, CT, USA, 2016.
(38) Schmidt, J. R.; Polik, W. F. *WebMO Enterprise*, Version 19.0, WebMO LLC: Madison, WI, USA, 2019. http://www.webmo.net (accessed Jan 2023).
(39) Stanton, J. F.; Gauss, J.; Harding, M. E.; Szalay, P. G.; with contributions from; Auer, A. A.; Bartlett, R. J.; Benedikt, U.; Berger, C.; Bernholdt, D. E.; Bomble, Y. J.; Cheng, L.; Christiansen, O.; Heckert,

https://doi.org/10.1021/acs.jpca.4c03093
J. Phys. Chem. A XXXX, XXX, XXX−XXX

M.; Heun, O.; Huber, C.; Jagau, T.-C.; Jonsson, D.; Jusélius, J.; Klein, K.; Lauderdale, W. J.; Lipparini, F.; Matthews, D. A.; Metzroth, T.; Mück, L. A.; O'Neill, D. P.; Price, D. R.; Prochnow, E.; Puzzarini, C.; Ruud, K.; Schiffmann, F.; Schwalbach, W.; Simmons, C.; Stopkowicz, S.; Tajti, A.; Vázquez, J.; Wang, F.; Watts, J. D.; and the integral packages MOLECULE; Almlöf, J.; Taylor, P. R.; PROPS; Taylor, P. R.; ABACUS; Helgaker, T.; Jensen, H. J. A.; Jørgensen, P.; Olsen, J.; and ECP routines by; Mitin, A. V.; van Wüllen, C. CFOUR, Coupled-Cluster Techniques for Computational Chemistry, v.2.0, 2014. http://www.cfour.de (accessed Jan 2023).

(40) Mills, I. M. Vibration-Rotation Structure in Asymmetric- and Symmetric-Top Molecules. In *Molecular Spectroscopy: Modern Research*; Rao, K. N.; Mathews, C. W., Eds.; Academic Press: New York, 1972; Vol. *1*, pp 115−140.

(41) Schneider, W.; Thiel, W. Anharmonic Force Fields from Analytic Second Derivatives: Method and Application to Methyl Bromide. *Chem. Phys. Lett.* **1989**, *157*, 367−373.

(42) Stanton, J. F.; Lopreore, C. L.; Gauss, J. The Equilibrium Structure and Fundamental Vibrational Frequencies of Dioxirane. *J. Chem. Phys.* **1998**, *108*, 7190−7196.

(43) Volka, K.; Adamek, P.; Stibor, I.; Ksandr, Z. Vibrational Spectra of 2- and 3-Furonitrile. *Spectrochim. Acta, Part A* **1976**, *32*, 397−401.

(44) Kisiel, Z.; Nixon, C. A.; Cordiner, M. A.; Thelen, A. E.; Charnley, S. B. Propionitrile in the Two Lowest Excited Vibrational States in the Laboratory and on Titan. *J. Mol. Spectrosc.* **2020**, *372*, No. 111324.

https://doi.org/10.1021/acs.jpca.4c03093
J. Phys. Chem. A XXXX, XXX, XXX−XXX